

# Theory of thermomagnonic torques in altermagnets

Edward Schwartz, Hamed Vakili, and Alexey A. Kovalev  
*Department of Physics and Astronomy and Nebraska Center for Materials and Nanoscience,  
 University of Nebraska, Lincoln, Nebraska 68588, USA*

We develop a theory of thermomagnonic torques in insulating altermagnets and predict a spin-splitter magnonic torque arising from the spin Seebeck effect. Additionally, we predict an anisotropic entropic torque. We study the effects of these torques on magnetic-texture dynamics and identify various anisotropic responses to temperature gradients. In particular, we predict spin-current-induced domain-wall precession, which can slow domain-wall motion for certain temperature-gradient directions. We also predict a temperature-gradient-driven anisotropic skyrmion Hall effect that enables fast skyrmion motion in response to thermal gradients. Our findings will be useful for spintronic applications such as magnetic racetrack memories and will serve as a hallmark of altermagnetism in insulating altermagnets with magnetic textures.

Altermagnets are a new class of materials that promise exceptional spintronic properties arising from unconventional time-reversal-symmetry breaking [1–7]. They can be characterized by spin symmetries that allow spin splitting of electronic bands, with  $d$ -,  $g$ -, or  $i$ -wave character depending on the material. Altermagnets combine useful properties of antiferromagnets (e.g., fast dynamics) with ferromagnet-like spin splitting and time-reversal-odd responses, enabling the crystal anomalous Hall effect [1, 8, 9], the spin-splitter effect [10–12], anisotropic magnon spectra with lifted degeneracy [13, 14], and spin currents induced by temperature gradients [15–19]. These and other useful features of altermagnets have driven rapid progress in recent years [20].

The dynamics of magnetic textures such as domain walls [21, 22] and skyrmions can be controlled by charge currents in altermagnets [23]. A potentially more energy-efficient approach is to use temperature gradients, as explored in spin caloritronics [24]. Altermagnets offer advantages for spin caloritronics because spin currents can be generated via the spin Seebeck effect without involving charge currents [15–18]. The angular momentum carried by magnons can be exploited to control magnetic textures, as it can exert spin-transfer torques on them [25–28]. A second mechanism for controlling magnetic textures is related to entropic forces that arise from gradients in temperature-dependent magnetic parameters, such as the exchange stiffness [26, 29–31].

In this paper, we develop a theory of thermomagnonic torques in insulating altermagnets. We apply our approach to a minimal model of a  $d$ -wave altermagnet [32] shown in Fig. 1; however, our theory can be readily generalized to other lattice models. We predict the existence of a spin-splitter thermomagnonic torque and show how it affects temperature-gradient-induced dynamics of magnetic textures. We also predict an anisotropic entropic torque that arises from the reduced symmetry of an altermagnet. We apply our theory to the dynamics of magnetic textures such as skyrmions and domain walls. The entropic torque drives domain walls and skyrmions toward the hot region. The magnonic spin-splitter torque

induces domain wall precession, thereby slowing motion for certain crystal alignments. We also predict a temperature-gradient-driven anisotropic skyrmion Hall effect arising from the magnonic spin-splitter torque, which enables fast skyrmion motion along a nanotrack in response to thermal gradients for certain crystal alignments.

*Thermomagnonic torques.* – We consider the stochastic Landau-Lifshitz-Gilbert (LLG) equation written on a lattice,

$$s(1 + \alpha \mathbf{S}_r \times) \partial_t \mathbf{S}_r = \frac{2}{v} \mathbf{S}_r \times \mathbf{h}_r, \quad (1)$$

where  $s = 2s_{\text{sub}}$  with  $s_{\text{sub}}$  being the spin density for one sublattice,  $v$  is the area/volume associated with a unit cell,  $\mathbf{r}$  denotes a site belonging to one of the two sublattices,  $\alpha$  stands for the Gilbert damping. The effective field  $\mathbf{h}_r$  is defined as  $\mathbf{h}_r = -\frac{\partial \mathcal{H}}{\partial \mathbf{S}_r} + \zeta_r$ . The stochastic field  $\zeta_r$  is defined using the relations

$$\langle \zeta_{\mathbf{r}_1}^\alpha(\omega) \zeta_{\mathbf{r}_2}^\beta(\omega') \rangle = \frac{2\pi \delta_{\alpha\beta} \alpha s_{\text{sub}} \hbar \omega}{\tanh(\hbar\omega/2T)} \delta_{\mathbf{r}_1 \mathbf{r}_2} \delta(\omega - \omega'). \quad (2)$$

We represent the unit vector  $\mathbf{S}_r$  entering Eq. (1) via two orthogonal components:  $\mathbf{S}_r = \sqrt{1 - (S_r^\perp)^2} \mathbf{S}_r^{(0)} + \mathbf{S}_r^\perp$ . The slowly varying component is represented by unit vector  $\mathbf{S}_r^{(0)}$  corresponds to a smooth magnetic texture while the fast component  $\mathbf{S}_r^\perp$  stands for a small deviation from  $\mathbf{S}_r^{(0)}$  caused by thermal field.

To identify thermomagnonic torques in Eq. (1), we concentrate on the transverse dynamics and split the fast and slow components in the LLG equation

$$s(1 + \alpha \chi_r \mathbf{S}_r^{(0)} \times) \partial_t \mathbf{S}_r^{(0)} = \frac{2}{v} \left[ \mathbf{S}_r^{(0)} \times \mathbf{h}_r^{(0)} \chi_r \right. \quad (3)$$

$$\left. - \sum_{\delta} J_{\delta} \mathbf{S}_r^{(0)} \times \mathbf{S}_{r+\delta}^{(0)} (\chi_{r+\delta} - \chi_r) \right], \quad (4)$$

$$\left. - \sum_{\delta} J_{\delta} \langle \mathbf{S}_r^\perp \times \mathbf{S}_{r+\delta}^\perp \rangle \right], \quad (5)$$

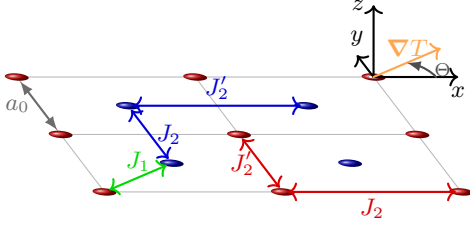


FIG. 1. A minimal model of a two-sublattice altermagnet. The two magnetic sublattices are shown as red and blue dots. The exchange interactions are indicated by double arrows. The unit cell, of area  $v = a_0^2$ , contains two magnetic sites. The temperature gradient  $\nabla T$  is applied at an angle  $\Theta$  with respect to the  $x$  axis.

where we use the exchange magnon approximation. Above,  $\mathbf{h}_r^{(0)} = -\frac{\partial \mathcal{H}}{\partial \mathbf{S}_r^{(0)}}$  is the effective field for  $\mathbf{S}_r^{(0)}$  calculated at zero temperature, and  $\chi_r = \langle \sqrt{1 - (S_r^\perp)^2} \rangle$  describes the shortening of the spin field.

We assume that the field  $\mathbf{S}_r^{(0)}$  varies slowly and can be represented by the Néel field  $\mathbf{n} = (\mathbf{S}_A^{(0)} - \mathbf{S}_B^{(0)})/2$  where the index  $A$  ( $B$ ) stands for one of two sublattices. After rewriting Eq. (4) in terms of  $\mathbf{n}$ , we obtain the following expression for the torque density

$$\tau_m^0 = 2\mathbf{n} \times (\beta \mathbf{u}_0 \cdot \partial) \mathbf{n}, \quad (6)$$

$$\tau_n^0 = 2\mathbf{n} \times (\beta' \mathbf{u}'_0 \cdot \partial) \mathbf{n}, \quad (7)$$

where  $\beta \mathbf{u}_0 = (\hat{A}_0^A + \hat{A}_0^B) \cdot \partial \chi / (2s)$  and  $\beta' \mathbf{u}'_0 = (\hat{A}_0^A - \hat{A}_0^B) \cdot \partial \chi / (2s)$ . Here we define the zero temperature exchange stiffness calculated for sublattice  $A$  or  $B$

$$A_{0ij}^{A/B} = -\frac{1}{v} \sum_{\delta} \delta_i \delta_j \cdot J_{\delta} (\mathbf{S}_r^{(0)} \cdot \mathbf{S}_{r+\delta}^{(0)}). \quad (8)$$

Equation (8) is calculated in the absence of the magnetic texture, i.e.,  $\mathbf{S}_r^{(0)}$  and  $\mathbf{S}_{r+\delta}^{(0)}$  are either collinear or anti-collinear according to the classical ground state.

We rewrite Eq. (5) by separating each term in the sum into the longitudinal and transverse with respect to  $\mathbf{S}_r^{(0)} \times \mathbf{S}_{r+\delta}^{(0)}$  components. The transverse contributions can be rewritten as the magnonic spin-transfer torques [26]

$$\tau_m^{\text{st}} = (\mathbf{u}' \cdot \partial) \mathbf{n}, \quad (9)$$

$$\tau_n^{\text{st}} = (\mathbf{u} \cdot \partial) \mathbf{n}, \quad (10)$$

where  $\mathbf{u} = (\mathbf{j}_{(1)} + \mathbf{j}_{(2)})/(2s)$ ,  $\mathbf{u}' = (\mathbf{j}_{(1)} - \mathbf{j}_{(2)})/(2s)$ , and the spin current density is calculated for the first  $\mathbf{j}_{(1)}$  or the second  $\mathbf{j}_{(2)}$  sublattice site [31, 33]. The spin current density is defined as

$$\mathbf{j}_r = -\frac{1}{v} \sum_{\delta} \delta \cdot J_{\delta} (\mathbf{S}_r^{(0)} \cdot \langle \mathbf{S}_r^\perp \times \mathbf{S}_{r+\delta}^\perp \rangle), \quad (11)$$

and it is calculated in the absence of the magnetic texture. Assuming curricular magnons, the remaining longitudinal contributions in Eq. (5) can be combined with

Eqs. (6) and (7) after introducing the finite temperature exchange stiffness. We arrive at entropic torques

$$\tau_m^{\text{tot}} = \mathbf{n} \times (\beta \mathbf{u} \cdot \partial) \mathbf{n}, \quad (12)$$

$$\tau_n^{\text{tot}} = \mathbf{n} \times (\beta' \mathbf{u}' \cdot \partial) \mathbf{n}, \quad (13)$$

where we define the finite temperature exchange stiffness

$$A_{ij}^{A/B} = -\frac{1}{v} \sum_{\delta} \delta_i \delta_j \cdot J_{\delta} (\mathbf{S}_r \cdot \mathbf{S}_{r+\delta}). \quad (14)$$

and  $\beta \mathbf{u} = (\partial \hat{A}^A + \partial \hat{A}^B)/(2s)$  and  $\beta' \mathbf{u}'_0 = (\partial \hat{A}^A - \partial \hat{A}^B)/(2s)$ . The torque in Eq. (12) has been termed entropic torque in Ref. [29]. Here we identify the anisotropic entropic torque contribution arising due to the altermagnetic interaction.

Phenomenologically, the form of torques in Eqs. (9), (10), (12), and (13) agrees with the form presented in Ref. [23] after  $\nabla T$  is associated with the charge current  $\mathbf{j}_c$ . For altermagnet with  $d$ -wave symmetry in Fig. 1, the shape of the response tensors is such that  $\mathbf{u} \propto \hat{\sigma}_0 \cdot \nabla T$  and  $\mathbf{u}' \propto \hat{\sigma}_z \cdot \nabla T$  where  $\hat{\sigma}_0$  is a unit matrix and  $\hat{\sigma}_z$  is the Pauli matrix.

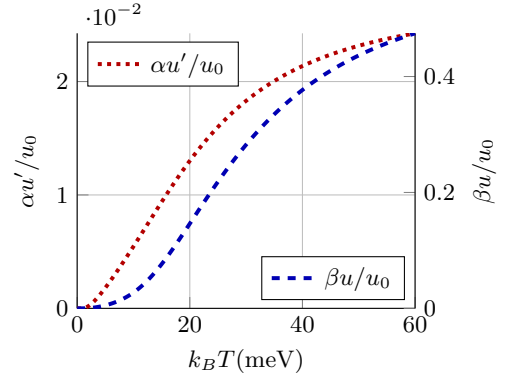


FIG. 2. Entropic and magnonic spin-splitter torques in an altermagnet, calculated using linear-response theory for the model in Eq. (15). Here  $u_0 = \nabla(k_B T)/s$ ,  $J_1 = 11.1$  meV,  $J_2 = -0.28$  meV,  $J'_2 = -3.48$  meV, and  $K = 0.047$  meV.

*Linear response calculations.* – For a model calculations of the spin-splitter magnonic and entropic torques, we consider a square lattice model of altermagnet in Fig. 1 with the Hamiltonian

$$\begin{aligned} \mathcal{H} = & J_1 \sum_{\langle i,j \rangle} \mathbf{S}_{ai} \cdot \mathbf{S}_{bj} + \sum_{\langle i_x, j_x \rangle} \left[ J_2 \mathbf{S}_{ai} \cdot \mathbf{S}_{aj} + J'_2 \mathbf{S}_{bi} \cdot \mathbf{S}_{bj} \right] \\ & + \sum_{\langle i_y, j_y \rangle} \left[ J'_2 \mathbf{S}_{ai} \cdot \mathbf{S}_{aj} + J_2 \mathbf{S}_{bi} \cdot \mathbf{S}_{bj} \right] - K \sum_{i,\mu=a,b} [(S_{\mu i}^z)^2], \end{aligned} \quad (15)$$

where indices  $a, b$  correspond to two sublattices. We perform the Holstein–Primakoff transformation to leading order in  $1/S$ . Within linear-response theory, the conventional spin-transfer torque coefficient  $\mathbf{u}$  vanishes. This,

however, does not mean that  $\beta\mathbf{u}$  vanishes, since  $\beta$  was introduced formally to allow comparison with Ref. [23]. The coefficient  $\mathbf{u}'$  is determined by the spin Seebeck effect [15] in a collinear configuration, i.e.,  $\mathbf{u}' = \mathbf{j}^s/s$ . For AFM alignment, we can define the Nambu spinor describing magnons,  $\Psi_{\mathbf{k}} = (\mathbf{a}_{\mathbf{k}}, \mathbf{a}_{-\mathbf{k}}^\dagger)^T$ , with  $\mathbf{a}_{\mathbf{k}} = (a_{\mathbf{k},1}, \dots, a_{\mathbf{k},N})^T$ . We also introduce the Hamiltonian

$$H = \frac{1}{2} \sum_{\mathbf{k}} \Psi_{\mathbf{k}}^\dagger \hat{H}_{\mathbf{k}} \Psi_{\mathbf{k}}, \quad \hat{H}_{\mathbf{k}} = \begin{pmatrix} h_{\mathbf{k}} & \Delta_{\mathbf{k}} \\ \Delta_{-\mathbf{k}}^\dagger & h_{-\mathbf{k}}^\dagger \end{pmatrix}, \quad (16)$$

with  $h_{\mathbf{k}} = h_{\mathbf{k}}^\dagger$  and  $\Delta_{\mathbf{k}} = \Delta_{-\mathbf{k}}^\dagger$  from hermiticity. The spin current is  $\mathbf{j}^s = \frac{1}{4} \Psi^\dagger(\mathbf{r}) (\hat{\mathbf{v}} \hat{\sigma}_3 \hat{S}_z + \hat{S}_z \hat{\sigma}_3 \hat{\mathbf{v}}) \Psi(\mathbf{r})$  where  $\hat{\sigma}_3$  describes the bosonic metric and  $\hat{S}_z$  is the spin operator [34, 35]. The paraunitary matrices  $T_{\mathbf{k}}$  diagonalize the Hamiltonian, i.e.,  $T_{\mathbf{k}}^\dagger \hat{H}_{\mathbf{k}} T_{\mathbf{k}} = E_{\mathbf{k}}$  with  $E_{\mathbf{k}} = (\varepsilon_{1\mathbf{k}}, \dots, \varepsilon_{N\mathbf{k}}, \varepsilon_{1,-\mathbf{k}}, \dots, \varepsilon_{N,-\mathbf{k}})$ . Defining the response coefficient as  $j_i^s = -\alpha_{ij}^s \nabla_j T$ , we obtain using linear response approach [36] for the spin current tensor

$$\alpha_{ij}^s = \frac{k_B \hbar}{2V} \sum_{n,\mathbf{k}} \frac{\mathcal{S}_{nn} v_{ni}(\mathbf{k}) v_{nj}(\mathbf{k}) \tau_{n\mathbf{k}}}{E_{n\mathbf{k}}} \Phi\left(\frac{E_{n\mathbf{k}}}{k_B T}\right), \quad (17)$$

where  $V$  is the volume/area of the system,  $\hat{\mathcal{S}} = \hat{\sigma}_3 T_{\mathbf{k}}^\dagger \hat{S}_z T_{\mathbf{k}}$  [36],  $\mathbf{v}_n = \frac{1}{\hbar} \partial_{\mathbf{k}} E_{n\mathbf{k}}$ ,  $\Phi(x) = x^2 e^x / (e^x - 1)^2$ , and  $\tau_{n\mathbf{k}}$  is the relaxation time. For altermagnet with  $d$ -wave symmetry, we recover the shape of the response tensor  $\hat{\alpha}^s = \alpha_0^s \hat{\sigma}_z$ , which agrees with symmetry analysis in Ref. [23]. The form of the scattering time  $\tau_{n\mathbf{k}}$  depends on the particular form of disorder. The result in Eq. (17) can be also obtained by solving the stochastic LLG equation for which the LLG phenomenology leads to  $\tau_{n\mathbf{k}} = \hbar / (2\varepsilon_{n\mathbf{k}} \alpha)$ .

Similarly, we obtain the gradient of the finite temperature exchange stiffness defined by the linear response equation  $\partial \hat{A}^{A/B} = -\eta^{A/B} \nabla T$  with

$$\eta^{A/B} = \frac{k_B}{2\mathcal{N}} \sum_{n,\mathbf{k}} \frac{\mathcal{A}_{nn}^{A/B}}{E_{n\mathbf{k}}} \Phi\left(\frac{E_{n\mathbf{k}}}{k_B T}\right), \quad (18)$$

where  $\mathcal{N}$  is the number of unit cells and  $\hat{A}^{A/B} = \hat{\sigma}_3 T_{\mathbf{k}}^\dagger \hat{A}_{\mathbf{k}}^{A/B} T_{\mathbf{k}}$ . Here  $\hat{A}_{\mathbf{k}}^{A/B}$  corresponds to the temperature dependent part of the exchange stiffness in Eq. (14) expressed in matrix form in terms of  $\Psi_{\mathbf{k}}$  after applying the Holstein-Primakoff transformation. For the model in Fig. 1, we have  $\hat{A}_{\mathbf{k}}^A + \hat{A}_{\mathbf{k}}^B = \partial \hat{H}_{\mathbf{k}} / \partial J_1 + 2\partial \hat{H}_{\mathbf{k}} / \partial J_2 + 2\partial \hat{H}_{\mathbf{k}} / \partial J'_2$ .

The results of our calculations are shown in Fig. 2, where we plot the magnitudes of the spin-splitter magnonic torque  $\mathbf{u}'$  and the entropic torque  $\beta\mathbf{u}$ . For the model in Eq. (15), we use the parameters  $J_1 = 11.1$  meV,  $J_2 = -0.28$  meV,  $J'_2 = -3.48$  meV, and  $K = 0.047$  meV. The results in Fig. 2 indicate that the spin-splitter torque should provide a sizable contribution to the dynamics of magnetic textures.

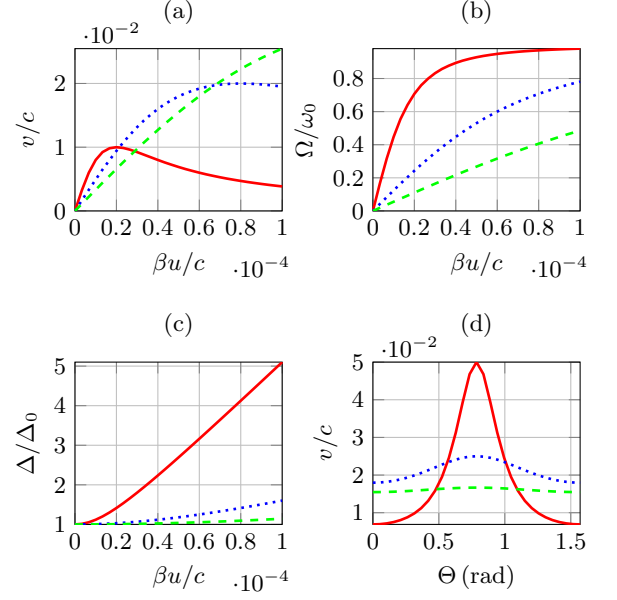


FIG. 3. (a) The domain wall velocity, (b) the angular precession speed  $\Omega$ , and (c) the domain wall width  $\Delta$  as a function of the strength of the entropic torque  $\beta u$  for  $\Theta = 0$ . (d) The domain wall velocity for different directions of the temperature gradient with respect to crystallographic axes described by  $\Theta$ . The magnonic spin transfer torque is chosen to roughly correspond to results in Fig. 2, i.e.,  $20\alpha\mathbf{u}' = \beta\mathbf{u}$ . The Gilbert damping is  $\alpha = 10^{-3}$  for the bold red,  $\alpha = 2 \cdot 10^{-3}$  for the dotted blue, and  $\alpha = 3 \cdot 10^{-3}$  for the dashed green curves.

*Dynamics of magnetic textures.* – Using the above calculated torques, we study the dynamics of domain walls in insulating altermagnets. We use the Lagrangian written for the staggered field [23]:

$$L = \frac{s}{2\omega_{\text{ex}}} \int \left[ \dot{\mathbf{n}}^2 - c^2 (\partial_{\alpha} \mathbf{n})^2 + \omega_0^2 n_z^2 + \mathbf{A} \cdot \dot{\mathbf{n}} + \mathbf{A}_{wz} (\mathbf{u}' \cdot \partial) \mathbf{n} \right] d^2 r, \quad (19)$$

where  $\mathbf{A} = \Lambda \mathbf{n} \times (\partial_x^2 \mathbf{n} - \partial_y^2 \mathbf{n})$  describes the altermagnetic interaction. In terms of the model in Fig. 1, we can write:  $\omega_{\text{ex}} = 16J_1/s$ ,  $c = (4/a_0) \sqrt{J_1(J_1 + 2J_2)/s^2}$ , and  $\omega_0 = (8/a_0^2) \sqrt{J_1 K/s^2}$ . The magnonic spin-splitter torque is included by adding a term containing the vector potential of the Wess-Zumino action  $\mathbf{A}_{wz}$ , i.e.,  $\nabla_{\mathbf{n}} \times \mathbf{A}_{wz} = 2\omega_{\text{ex}} \mathbf{n}$ . The entropic torques in Eqs. (12) and (13) are included via the Rayleigh function:

$$\mathcal{R} = s \left[ \frac{\alpha \dot{\mathbf{n}}^2}{2} + \dot{\mathbf{n}} \cdot (\beta \mathbf{u}' \cdot \partial) \mathbf{n} + \dot{\mathbf{m}} \cdot (\beta' \mathbf{u}' \cdot \partial) \mathbf{n} \right], \quad (20)$$

where  $\alpha$  is the Gilbert damping parameter. Note that the Euler-Lagrange-Rayleigh equation derived from Eqs. (20) yields an additional higher-order torque term,  $\boldsymbol{\tau}_m = \mathbf{m} \times [\beta' \mathbf{u}' \cdot \partial] \mathbf{n}$ . For convenience in what follows we use spherical coordinates, i.e.,  $\mathbf{n} = (\sin \theta \cos \phi, \cos \theta \sin \phi, \cos \theta)$ .

To study the domain wall dynamics, we use the following ansatz describing the domain wall profile [21, 23, 37],  $\cos \theta(x, t) = \pm \tanh \frac{x - X(t)}{\Delta(t)}$ , and  $\phi(x, t) = \Phi(t) + b(t) \frac{x - X(t)}{\Delta(t)}$  with  $X(t)$  and  $\Phi(t)$  being the collective variables that describe the position and the tilt. The collective variables  $b(t)$  and  $\Delta(t)$  are treated as slow variables. From the equations of motion, we find the slow variables  $\Delta = \Delta_0 [1 - v^2/c^2]/\sqrt{1 - v^2/c^2 - \Omega^2/\omega_0^2}$  and  $b = \Delta v \Omega/(c^2 - v^2)$  where  $\Delta_0 = c/\omega_0$  is the width of the equilibrium domain wall,  $v = \dot{X}$ , and  $\Omega = \dot{\Phi}$ . The equations of motion become

$$\ddot{X}/\omega_{\text{ex}} = \beta u - \alpha \dot{X} - bu', \quad (21)$$

$$\ddot{\Phi}/\omega_{\text{ex}} = \frac{u'}{\Delta}(1 + b^2) - \alpha \dot{\Phi}, \quad (22)$$

where we dropped the higher order term proportional to  $\beta' u'$  and describing the anisotropic entropic torque.

In Fig. 3, we plot the results of Eqs. (21) and (22) for different values of the Gilbert damping. In Fig. 3(a) and (b), we observe that smaller Gilbert damping leads to faster domain-wall precession, which in turn slows the domain-wall motion. The precession originates from angular-momentum conservation: the angular momentum carried by magnons is absorbed by the lattice via domain-wall precession. In Fig. 3(c), we observe that the domain-wall width increases, in contrast to the Lorentz contraction typical of antiferromagnets. In Fig. 3(d), we observe anisotropy in the domain-wall speed for different temperature gradient directions relative to the crystallographic axes, parameterized by  $\Theta$ . For  $\Theta = \pi/4$ , the spin current does not transfer angular momentum to the domain wall, and fast domain-wall motion is restored.

To study skyrmion dynamics, we assume that the skyrmion texture is stabilized—for example, by the presence of an interfacial Dzyaloshinskii–Moriya interaction (DMI), which was taken to be  $0.35 \text{ mJ/m}^2$  for the model in Eq. (15). We assume a traveling-wave solution of the form  $\mathbf{n}(\mathbf{r} - \mathbf{v}t)$ . For velocities much smaller than  $c$ , we employ a  $360^\circ$  domain-wall ansatz [38–40], while at larger velocities we use a deformed “relativistic” skyrmion profile [41, 42]. The skyrmion position is parameterized by the generalized coordinate  $\mathbf{X}(t)$ , which yields the Thiele equation after substituting the skyrmion ansatz into the Lagrangian (19):

$$\hat{\mathcal{M}} \ddot{\mathbf{X}} + \hat{\mathcal{G}} \dot{\mathbf{X}} + \alpha \hat{\mathcal{D}} \dot{\mathbf{X}} + \hat{\mathcal{B}} \dot{\mathbf{X}} = \mathbf{F}, \quad (23)$$

where  $\hat{\mathcal{M}}$  is the skyrmion mass tensor,  $\hat{\mathcal{G}}$  is the antisymmetric gyrotensor,  $\mathcal{D}_{ij} = \int d^2r (\partial_i \mathbf{n} \cdot \partial_j \mathbf{n})$  is the dissipative tensor, and  $\mathcal{B}_{ij} = \int d^2r [\partial_i (\mathbf{A} \cdot \partial_j \mathbf{n}) - \partial_j (\mathbf{A} \cdot \partial_i \mathbf{n})]$  arises from the altermagnetic term in the Lagrangian. Here we consider a compensated antiferromagnet, for which the gyrotensor vanishes. For the force we obtain

$$\mathbf{F} = 4\pi \hat{\mathbf{z}} \times \mathbf{u}' + \hat{\mathcal{D}} \cdot (\beta \mathbf{u}), \quad (24)$$

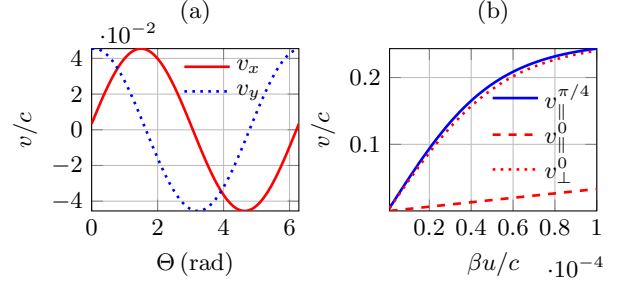


FIG. 4. (a) Components of the skyrmion velocity,  $v_x$  and  $v_y$ , for different directions of the temperature gradient  $\nabla T$  with respect to the crystallographic axes, parameterized by  $\Theta$ . The temperature gradient corresponds to  $\beta u/c = 10^{-5}$ . (b) Skyrmion velocity component parallel ( $v_{\parallel}$ ) and perpendicular ( $v_{\perp}$ ) to  $\nabla T$  as a function of the strength of the entropic torque  $\beta u$ . The results are shown for  $\Theta = 0$  and  $\Theta = \pi/4$ . Since  $v_{\perp}^{\pi/4} = 0$ , the corresponding curve is not shown. In all plots, the magnonic spin-transfer torque is chosen to roughly match the results in Fig. 2, i.e.,  $20\alpha u' = \beta u$ . The Gilbert damping is  $\alpha = 3 \times 10^{-3}$ .

where we neglect the higher-order term proportional to  $\beta' \mathbf{u}'$  that describes the anisotropic entropic torque. Because of the spin-splitter magnonic torque, the force is not aligned with the temperature gradient, and we expect a temperature-gradient-induced skyrmion Hall effect. The steady-state skyrmion velocity then reads

$$\mathbf{v} = \frac{\beta \mathbf{u}}{\alpha} + \frac{4\pi}{\alpha |\hat{\mathcal{D}}|} \hat{\mathbf{z}} \times (\hat{\mathcal{D}} \mathbf{u}'), \quad (25)$$

where  $|\hat{\mathcal{D}}| = \det \hat{\mathcal{D}}$ . We also neglect the  $\hat{\mathcal{B}}$  term, whose effect is small unless the skyrmion profile is strongly deformed [23].

In Fig. 4(a), we plot components of the skyrmion velocity,  $v_x$  and  $v_y$  from Eq. (25), for different directions of the temperature gradient  $\nabla T$  with respect to the crystallographic axes, parameterized by  $\Theta$ . The spin-splitter magnonic torque leads to the anisotropic skyrmion Hall effect. Interestingly, for the alignment corresponding to  $\Theta = \pi/4$  we observe no side motion of skyrmion as can be seen in Fig. 4(b). This fast motion along the temperature gradient is mostly induced by the spin-splitter magnonic torque and can be useful for applications.

*Conclusions.* — We have formulated a theory of thermomagnonic torques applicable to a general lattice model and applied it to insulating altermagnets. We have identified entropic torques that drive magnetic textures toward the hot region in response to a temperature gradient. Owing to the reduced symmetry of an altermagnet, we also identify an anisotropic entropic torque. In addition, we identify a magnonic spin-splitter torque that induces domain-wall precession for certain crystal alignments and leads to a temperature-gradient-induced anisotropic skyrmion Hall effect. The latter can be particularly useful for racetrack memories, as it enables fast

motion along a nanotrack driven by the magnonic spin-splitter torque without transverse deflection for appropriately engineered crystal alignments. We note that for sharp magnetic textures, additional effects related to linear-momentum transfer need to be included [43, 44]. Our results demonstrate that altermagnets exhibit certain properties of ferromagnets and ferrimagnets while retaining useful properties of conventional antiferromagnets. These findings can serve as a hallmark of altermagnetism in insulating altermagnets with magnetic textures.

*Acknowledgments.* – This work was supported by the U.S. Department of Energy, Office of Science, Basic Energy Sciences, under Award No. DE-SC0021019.

---

[1] L. Šmejkal, R. Gonzalez-Hernandez, T. Jungwirth, and J. Sinova, Crystal time-reversal symmetry breaking and spontaneous hall effect in collinear antiferromagnets, *Sci. Adv.* **6**, eaaz8809 (2020).

[2] M. Naka, S. Hayami, H. Kusunose, Y. Yanagi, Y. Motome, and H. Seo, Spin current generation in organic antiferromagnets, *Nat. Commun.* **10**, 4305 (2019).

[3] L.-D. Yuan, Z. Wang, J.-W. Luo, E. I. Rashba, and A. Zunger, Giant momentum-dependent spin splitting in centrosymmetric low- $z$  antiferromagnets, *Phys. Rev. B* **102**, 014422 (2020).

[4] M. Naka, Y. Motome, and H. Seo, Perovskite as a spin current generator, *Phys. Rev. B* **103**, 125114 (2021).

[5] Y. Guo, H. Liu, O. Janson, I. C. Fulga, J. van den Brink, and J. I. Facio, Spin-split collinear antiferromagnets: A large-scale ab-initio study, *Mater. Today Phys.* **32**, 100991 (2023).

[6] L. Šmejkal, J. Sinova, and T. Jungwirth, Emerging research landscape of altermagnetism, *Phys. Rev. X* **12**, 040501 (2022).

[7] L. Šmejkal, J. Sinova, and T. Jungwirth, Beyond conventional ferromagnetism and antiferromagnetism: A phase with nonrelativistic spin and crystal rotation symmetry, *Phys. Rev. X* **12**, 031042 (2022).

[8] L. Šmejkal, A. H. MacDonald, J. Sinova, S. Nakatsuji, and T. Jungwirth, Anomalous hall antiferromagnets, *Nat. Rev. Mater.* **7**, 482 (2022).

[9] T. Sato, S. Haddad, I. C. Fulga, F. F. Assaad, and J. van den Brink, Altermagnetic anomalous hall effect emerging from electronic correlations, *Phys. Rev. Lett.* **133**, 086503 (2024).

[10] M. Naka, S. Hayami, H. Kusunose, Y. Yanagi, Y. Motome, and H. Seo, Spin current generation in organic antiferromagnets, *Nat. Commun.* **10**, 4305 (2019).

[11] R. González-Hernández, L. Šmejkal, K. Výborný, Y. Yanagi, J. Sinova, T. c. v. Jungwirth, and J. Železný, Efficient electrical spin splitter based on nonrelativistic collinear antiferromagnetism, *Phys. Rev. Lett.* **126**, 127701 (2021).

[12] H. Bai, L. Han, X. Y. Feng, Y. J. Zhou, R. X. Su, Q. Wang, L. Y. Liao, W. X. Zhu, X. Z. Chen, F. Pan, X. L. Fan, and C. Song, Observation of spin splitting torque in a collinear antiferromagnet ruo<sub>2</sub>, *Phys. Rev. Lett.* **128**, 197202 (2022).

[13] L. Šmejkal, A. Marmodoro, K.-H. Ahn, R. González-Hernández, I. Turek, S. Mankovsky, H. Ebert, S. W. D’Souza, O. c. v. Šipr, J. Sinova, and T. c. v. Jungwirth, Chiral magnons in altermagnetic ruo<sub>2</sub>, *Phys. Rev. Lett.* **131**, 256703 (2023).

[14] M. Gohlke, A. Corticelli, R. Moessner, P. A. McClarty, and A. Mook, Spurious symmetry enhancement in linear spin wave theory and interaction-induced topology in magnons, *Phys. Rev. Lett.* **131**, 186702 (2023).

[15] Q. Cui, B. Zeng, P. Cui, T. Yu, and H. Yang, Efficient spin seebeck and spin nernst effects of magnons in altermagnets, *Phys. Rev. B* **108**, L180401 (2023).

[16] M. Weißenhofer and A. Marmodoro, Atomistic spin dynamics simulations of magnonic spin seebeck and spin nernst effects in altermagnets, *Phys. Rev. B* **110**, 094427 (2024).

[17] K. V. Yershov, V. P. Kravchuk, M. Daghofer, and J. van den Brink, Fluctuation-induced piezomagnetism in local moment altermagnets, *Phys. Rev. B* **110**, 144421 (2024).

[18] K. Wu, J. Dong, M. Zhu, F. Zheng, and J. Zhang, Magnon splitting and magnon spin transport in altermagnets, *Chin. Phys. Lett.* **42**, 070702 (2025).

[19] E. Galindez-Ruales, W. Yang, T. Dannegger, M. Kundu, J. Köhler, C. Schmitt, F. Fuhrmann, A. Akashdeep, D. M. Tran, X. Ma, G. Jakob, S. Cao, U. Nowak, and M. Kläui, *Altermagnetic magnon transport in the d-wave altermagnet lufeo<sub>3</sub>*, arXiv preprint (2025), arXiv:2508.14569v2, arXiv:2508.14569 [cond-mat.mtrl-sci].

[20] T. Jungwirth, J. Sinova, P. Wadley, D. Kriegner, H. Reichlová, F. Křížek, H. Ohno, and L. Šmejkal, *Altermagnetic spintronics*, arXiv preprint (2025), arXiv:2508.09748 [cond-mat.mtrl-sci].

[21] O. Gomonay, V. P. Kravchuk, R. Jaeschke-Ubiergo, K. V. Yershov, T. Jungwirth, L. Šmejkal, J. van den Brink, and J. Sinova, Structure, control, and dynamics of altermagnetic textures, *npj Spintronics* **2**, 35 (2024).

[22] V. P. Kravchuk, K. V. Yershov, J. I. Facio, Y. Guo, O. Janson, O. Gomonay, J. Sinova, and J. van den Brink, Chiral magnetic excitations and domain textures of g-wave altermagnets, *Phys. Rev. B* **112**, 144421 (2025).

[23] H. Vakili, E. Schwartz, and A. A. Kovalev, Spin-transfer torque in altermagnets with magnetic textures, *Phys. Rev. Lett.* **134**, 176401 (2025).

[24] T. Kikkawa and E. Saitoh, Spin seebeck effect: Sensitive probe for elementary excitation, spin correlation, transport, magnetic order, and domains in solids, *Annu. Rev. Condens. Matter Phys.* **14**, 129 (2023).

[25] P. Yan, X. S. Wang, and X. R. Wang, All-magnonic spin-transfer torque and domain wall propagation, *Phys. Rev. Lett.* **107**, 177207 (2011).

[26] A. A. Kovalev and Y. Tserkovnyak, Thermomagnonic spin transfer and peltier effects in insulating magnets, *EPL (Europhysics Letters)* **97**, 67002 (2012).

[27] X.-g. Wang, G.-h. Guo, Y.-z. Nie, G.-f. Zhang, and Z.-x. Li, Domain wall motion induced by the magnonic spin current, *Phys. Rev. B* **86**, 054445 (2012).

[28] D. Hinzke and U. Nowak, Domain wall motion by the magnonic spin seebeck effect, *Phys. Rev. Lett.* **107**, 027205 (2011).

[29] F. Schlickeiser, U. Ritzmann, D. Hinzke, and U. Nowak, Role of entropy in domain wall motion in thermal gradi-

ents, *Phys. Rev. Lett.* **113**, 097201 (2014).

[30] S. Selzer, U. Atxitia, U. Ritzmann, D. Hinzke, and U. Nowak, Inertia-free thermally driven domain-wall motion in antiferromagnets, *Phys. Rev. Lett.* **117**, 107201 (2016).

[31] S. K. Kim and Y. Tserkovnyak, Landau-lifshitz theory of thermomagnonic torque, *Phys. Rev. B* **92**, 020410 (2015).

[32] B. Brekke, A. Brataas, and A. Sudbø, Two-dimensional altermagnets: Superconductivity in a minimal microscopic model, *Phys. Rev. B* **108**, 224421 (2023).

[33] A. A. Kovalev, Skyrmionic spin seebeck effect via dissipative thermomagnonic torques, *Phys. Rev. B* **89**, 241101 (2014).

[34] V. A. Zyuzin and A. A. Kovalev, Magnon spin nernst effect in antiferromagnets, *Phys. Rev. Lett.* **117**, 217203 (2016).

[35] B. Li, S. Sandhoefner, and A. A. Kovalev, Intrinsic spin nernst effect of magnons in a noncollinear antiferromagnet, *Phys. Rev. Res.* **2**, 013079 (2020).

[36] B. Li, A. Mook, A. Raeliarijaona, and A. A. Kovalev, Magnonic analog of the edelstein effect in antiferromagnetic insulators, *Phys. Rev. B* **101**, 024427 (2020).

[37] A. Kosevich, B. Ivanov, and A. Kovalev, Magnetic solitons, *Phys. Rep.* **194**, 117–238 (1990).

[38] F. Büttner, I. Lemesh, and G. S. D. Beach, Theory of isolated magnetic skyrmions: From fundamentals to room temperature applications, *Sci. Rep.* **8**, 4464 (2018).

[39] X. S. Wang, H. Y. Yuan, and X. R. Wang, A theory on skyrmion size, *Commun. Phys.* **1**, 31 (2018).

[40] H.-B. Braun, Fluctuations and instabilities of ferromagnetic domain-wall pairs in an external magnetic field, *Phys. Rev. B* **50**, 16485 (1994).

[41] E. A. Tremsina and G. S. D. Beach, Atomistic simulations of distortion-limited high-speed dynamics of antiferromagnetic skyrmions, *Phys. Rev. B* **106**, L220402 (2022).

[42] S. Komineas and N. Papanicolaou, Traveling skyrmions in chiral antiferromagnets, *SciPost Phys.* **8**, 086 (2020).

[43] S. K. Kim, Y. Tserkovnyak, and O. Tchernyshyov, Propulsion of a domain wall in an antiferromagnet by magnons, *Phys. Rev. B* **90**, 104406 (2014).

[44] P. Shen, Y. Tserkovnyak, and S. K. Kim, Driving a magnetized domain wall in an antiferromagnet by magnons, *J. Appl. Phys.* **127**, 223905 (2020).